Nanoscale Res Lett (2009) 4:197–203
DOI 10.1007/s11671-008-9225-2

NANO EXPRESS

Effect of Growth Temperature on Bamboo-shaped Carbon–Nitrogen (C–N) Nanotubes Synthesized Using Ferrocene Acetonitrile Precursor

Ram Manohar Yadav · Pramod Singh Dobal · T. Shripathi · R. S. Katiyar · O. N. Srivastava

Received: 7 October 2008 / Accepted: 24 November 2008 / Published online: 10 December 2008

Abstract This investigation deals with the effect of growth temperature on the microstructure, nitrogen content, and crystallinity of C–N nanotubes. The X-ray photoelectron spectroscopic (XPS) study reveals that the atomic percentage of nitrogen content in nanotubes decreases with an increase in growth temperature. Transmission electron microscopic investigations indicate that the bamboo compartment distance increases with an increase in growth temperature. The diameter of the nanotubes also increases with increasing growth temperature. Raman modes sharpen while the normalized intensity of the defect mode decreases almost linearly with increasing growth temperature. These changes are attributed to the reduction of defect concentration due to an increase in crystal planar domain sizes in graphite sheets with increasing temperature. Both XPS and Raman spectral observations indicate that the C–N nanotubes grown at lower temperatures possess higher degree of disorder and higher N incorporation.

R. M. Yadav · O. N. Srivastava
Department of Physics, Banaras Hindu University, Varanasi 221005, India

R. M. Yadav (✉) · P. S. Dobal
Department of Physics, VSSD College, Kanpur 208002, India
e-mail: rmanohar28@yahoo.co.in

T. Shripathi
UGC-DAE Consortium for Scientific Research, University Campus, Khandwa Road, Indore 452017, India

R. S. Katiyar
Department of Physics, University of Puerto Rico, San Juan, PR, USA

Keywords Carbon nitrogen (C–N) nanotubes · Bamboo-shaped nanotubes · Spray pyrolysis

Introduction

Hollow and porous structures, such as nanotubes of carbon and other inorganic materials, have emerged as an intriguing class of nanomaterials due to their widespread novel properties and applications [1–8]. Doped carbon nanotubes have also attracted considerable attention owing to their outstanding properties [9–14]. Among various doped nanotubes, nitrogen-doped carbon (C–N) nanotubes exhibit novel electronic, chemical, and mechanical properties that are not found in pure carbon nanotubes [15]. To exploit these novel properties fully, low dopant concentrations were incorporated within these tubes [16]. Using such low concentration, the electronic conductance would be significantly enhanced without altering mechanical properties [17]. In addition, because of the presence of donors in N-doped nanotubes, their surface would become more reactive [18]. This reactivity would be extremely useful in the development of field-emission sources, nanoelectronics, sensors, and strong composite materials.

In order to exploit curious properties, it is essential to develop synthesis methods, which are capable of producing C–N nanotubes of specific length preferably in aligned configurations. Regarding synthesis, chemical vapor deposition (CVD) is the simplest yet effective technique for the formation of CNTs and C–N nanotubes. The understanding of the mechanisms involved in the growth of CNTs by CVD is a critical point. It needs to be elucidated as how to control the degree of growth necessary for many envisaged applications of CNTs. There are a plethora of experimental parameters that need to be taken into account

along the basic knowledge about the way they influence each other. One crucial parameter is the shape and chemical state of the catalytic particle employed. In the case of growth directly on substrates, these two factors are strongly dependent on the nature of the selected substrate [19]. On the basis of numerous trial-and-error studies published in the literature, there is a clear consensus on the importance of selecting the appropriate catalyst–substrate combination. However, there remains a high degree of confusion regarding the exact role played by the chemical composition and structure of the catalytic particles since the precise CNT growth mechanism is mostly unknown. Additional problems arise due to high temperatures and aggressive gas environments associated with the CVD process—the initial shape and chemical composition of the catalyst changes in a complex way [20]. The influence of the oxidation state of the catalyst for CNT growth has been investigated recently [21–23]. However, a controversial point in such cases is that the chemical analysis is performed ex situ with the consequent modification of the original composition due to exposure to air, which makes interpretation of the data difficult. Investigations of the growth of CNT by metal-catalyzed CVD have generally found that, under any given conditions, there exist some maximum lengths to which the CNT can be grown. Detailed studies of CNT length versus growth time generally have shown that at any given temperature CNTs grow at an approximately constant rate for a certain period of time (which depends on CVD conditions) after which growth ceases [24–33]. CNT nucleation and growth are generally believed to occur when a catalytic metal sample forms nanometer-sized particles at elevated temperatures and then C_2H_4 or other carbon feedstock molecules decompose upon these particles to release their carbon atoms. If the particle is in the correct size range, the carbon atoms arrange themselves into a cylinder of concentric carbon shells that grows away from the catalytic particle as a carbon nanotube. CNT growth stops when the catalytic particle becomes deactivated. Possible mechanisms for this deactivation include over coating with carbon and conversion of the metal into metal carbide or other noncatalytic forms. Whatever may be the mechanism, the cessation of growth after a relatively short time, with corresponding short maximum length of producible CNTs, clearly limits the utility of CNTs in many materials applications. Hence, an understanding of the mechanism(s), CNT growth cessation as well as the influence of other process parameters is necessary. Keeping these aspects in view, we have synthesized bamboo-shaped C–N nanotube bundles by spray pyrolysis of ferrocene–acetonitrile solution. This study focuses on the effect of variation of growth temperature on the microstructural features, nitrogen concentration, and the crystallinity of the nanotubes and the inter-relationship of these features.

Experimental Details

The details about the experimental set-up of spray pyrolysis have already been given in our previous publications [34, 35]. It may be mentioned that whereas ferrocene contains carbon and iron, the solvent acetonitrile contains nitrogen, carbon, and hydrogen. Varying the concentration of ferrocene in a given volume of acetonitrile automatically changes the nitrogen concentration in the solution and hence in the as-grown CNTs. All the experiments have been performed at the optimum flowrate of 2 mL/min. For this investigation, we choose ferrocene–acetonitrile as a precursor at 5 mg/mL concentration of ferrocene in acetonitrile while keeping all the other experimental parameters constant. The syntheses of C–N nanotubes have been done at 850, 900, and 950 °C. The as synthesized product was taken out and characterized by using scanning electron microscopic (SEM) (Philips, XL-20), transmission electron microscopic (TEM), and X-ray photoelectron spectroscopic (XPS) techniques. Philips EM CM-12 was used for TEM measurements, whereas the X-ray photoelectron spectrum was recorded in VSW ESCA instrument (using Al K_α radiation with a total resolution $\sim$0.9 eV at 2×10^{-9} torr base vacuum). The unpolarized Raman spectra of the C–N nanotube samples were recorded in back scattering geometry using a micro-Raman set-up (Jobin-Yvon, Model T64000) consisting of a Microscope (Olympus) with an 80× objective, triple-monochromator, and a charge-coupled device (CCD) multi-channel detector. Samples were excited with 514.5 nm line from an Ar-ion laser (Coherent, Model Innova 90). With a 25-mm CCD and 1800 grooves/mm grating, the spectral resolution was typically <1 cm^{-1}. Our observations indicated that the C–N nanotubes that grown at lower temperature possess higher degree of disorder and higher N incorporation.

Results and Discussion

Microstructural Analysis

SEM exploration revealed the formation of clean, well-aligned C–N nanotube bundles at all the growth temperatures. A representative SEM micrograph is shown in Fig. 1a, which clearly shows the formation of nanotube bundles having length of about 430 μm. Figure 1b is the magnified image of a nanotubes bundle shown in Fig. 1a, which clearly exhibits that the as-grown nanotubes do not contain any impurities traces like amorphous and vitreous carbon. It is also clear from this micrograph that the nanotubes are in aligned fashion.

TEM investigations reveal the variation in microstructure of C–N nanotubes synthesized at different

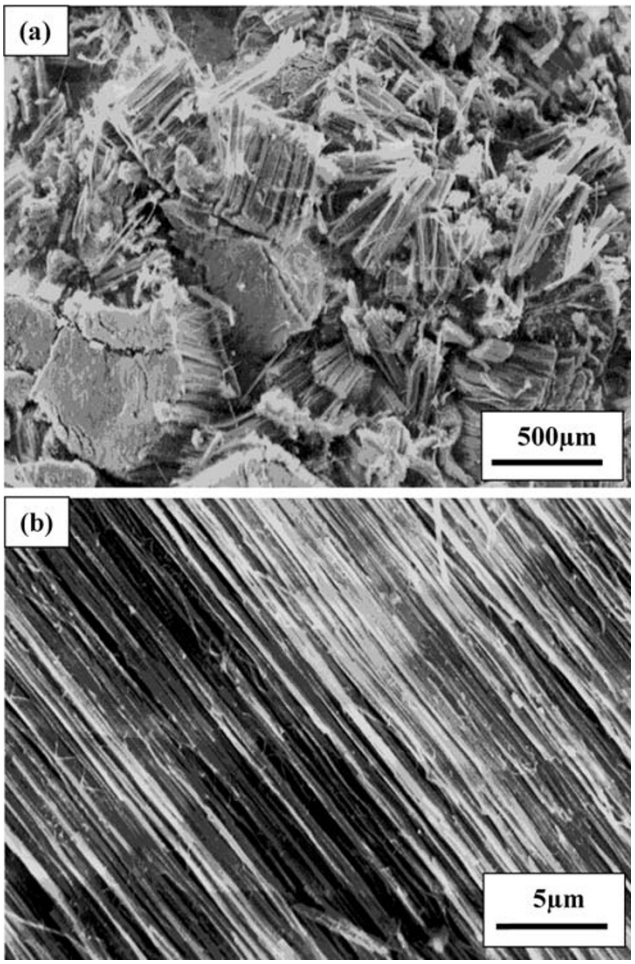

Fig. 1 **a** SEM image of large area of as-grown nanotubes/nanotubes bundles; **b** the magnified image of a nanotubes bundle as shown in (**a**)

temperatures. The TEM micrographs, as shown in Fig. 2a–c, clearly illustrated that the C–N nanotubes were of a bamboo-shaped structure for all temperatures. The average diameters of nanotubes are about 55, 60, and 73 nm, respectively, at 850, 900, and 950 °C. The average diameter of the nanotubes slightly increases with increase in growth temperature in the range of 850 to 950 °C as shown in Fig. 2. The diameter distribution of these C–N nanotubes obtained from the TEM analysis is represented qualitatively in Fig. 3. As the growth temperature increases more agglomeration occurs, resulting in a larger-sized catalyst particles and therefore larger diameter nanotubes were obtained. Similar observations on C–N nanotubes have been made by using other precursors [31, 36]. The compartment distance also increases with increase in growth temperature. As the temperature increases, the nitrogen content decreases and results in increased compartment separation. The increased compartment distance with decreasing nitrogen concentration results from the enhancement in the number of compartment layers with nitrogen incorporation as also suggested by Jang et al. [37].

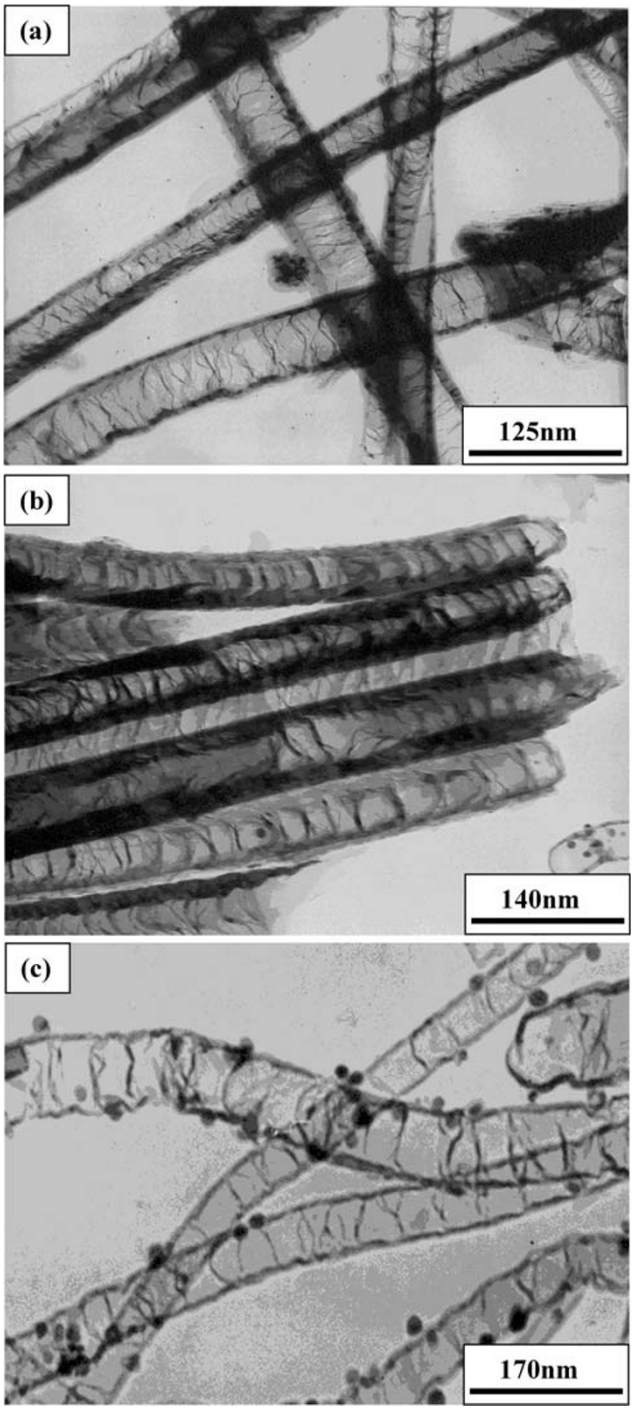

Fig. 2 TEM images of nanotubes grown at **a** 850 °C, **b** 900 °C, and **c** 950 °C temperatures

XPS Analysis

Figure 4 shows the XPS spectrum of C–N nanotubes. Figure 4a shows the C 1s peaks at 284.2 eV and Fig. 4b shows the N 1s peaks at ∼401 eV, at different growth temperatures. The percentage (atomic) nitrogen content in

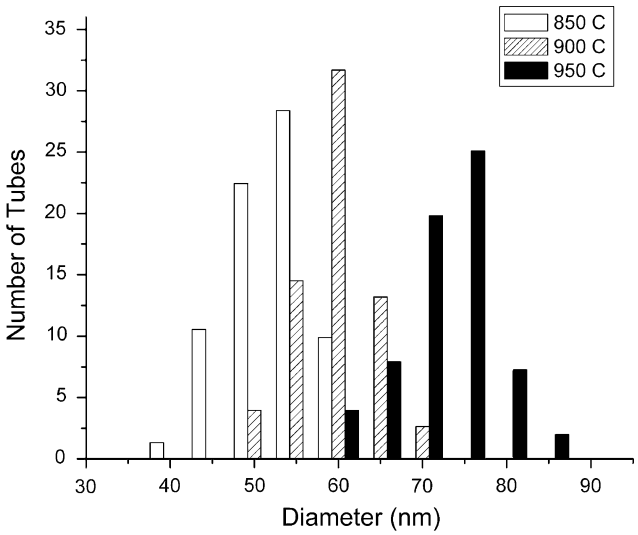

Fig. 3 The diameter distribution of C–N nanotubes synthesized at three different temperatures

the nanotubes decreases with increase in growth temperature, as shown in Fig. 4c. The percentage (atomic) nitrogen contents present in the nanotubes are 8.29, 4.65, and 3.19% for 850, 900, and 950 °C, respectively, and their relative composition comes out to be $C_{11}N$, $C_{23}N$, and $C_{30}N$. van Dommele et al. [38] have reported the tuning nitrogen functionalities in catalytically grown nitrogen-containing carbon nanotubes as well as the influence of growth temperature on nitrogen content. Our results corroborate their findings of an increase in C/N ratio with increasing temperature. Based on the TEM and XPS investigations, it is apparent that the increases in the bamboo compartment distance of the C–N nanotubes are due to the decreased nitrogen content in C–N nanotubes with increase in temperature. Earlier we have shown that in our case the base growth mechanism is the most favored mechanism in the formation of bamboo-shaped C–N nanotubes [34, 35]. In the base growth model, C and N incorporation results in the walls being pushed away from the stationary catalyst to form the tubular structure. The nucleation and growth of CNT follow the adsorption–decomposition-surface diffusion-bulk diffusion–nucleation process [39]. Nitrogen plays the key role in compartment generation by the formation of pentagons in addition to hexagons [40] and also by increasing the bulk diffusion of carbon and nitrogen species in catalyst nanoparticles [41]. As the growth temperature increases, consequently the nitrogen concentration in the nanotubes decreases, and therefore compartment layers are formed at longer distances. This could be the reason for an increase in the compartment distances with increasing growth temperature.

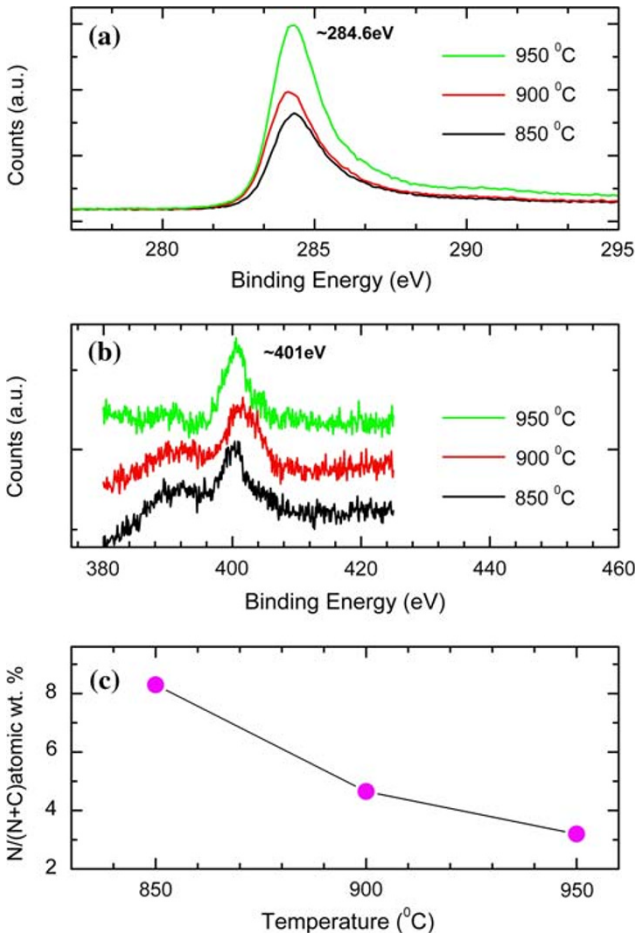

Fig. 4 XPS spectra of C–N nanotubes grown at different temperatures; **a** C 1s spectra, **b** N 1s spectra, and **c** variation of nitrogen content in nanotubes with growth temperature

Raman Spectroscopic Analysis

Raman spectroscopy has been applied for the identification and characterization of a wide variety of nano-structured materials [42–46] and has been shown to be a perfect tool to evaluate the crystallinity and the defects in carbon structures [47] as well as to analyze the behavior of carbon nanoparticles embedded in different matrices [48]. Raman spectra of the C–N nanotubes that grown at different temperatures are shown in Fig. 5. The strong band around 1585 cm^{-1}, which is referred to as the G-band, is usually regarded as a Raman-allowed G-point vibration corresponding to the optical phonon modes of E_{2g} symmetry in graphite and often called tangential mode for carbon nanotubes [42, 43]. The D-band at around 1351 cm^{-1}, which originates from defects in the curved graphene sheets, tube ends, or from the presence of carbon coating on the outside of the tubular bands [44], is associated with optical phonons close to the K-point of the Brillouin zone in graphite and carbon nanotubes.

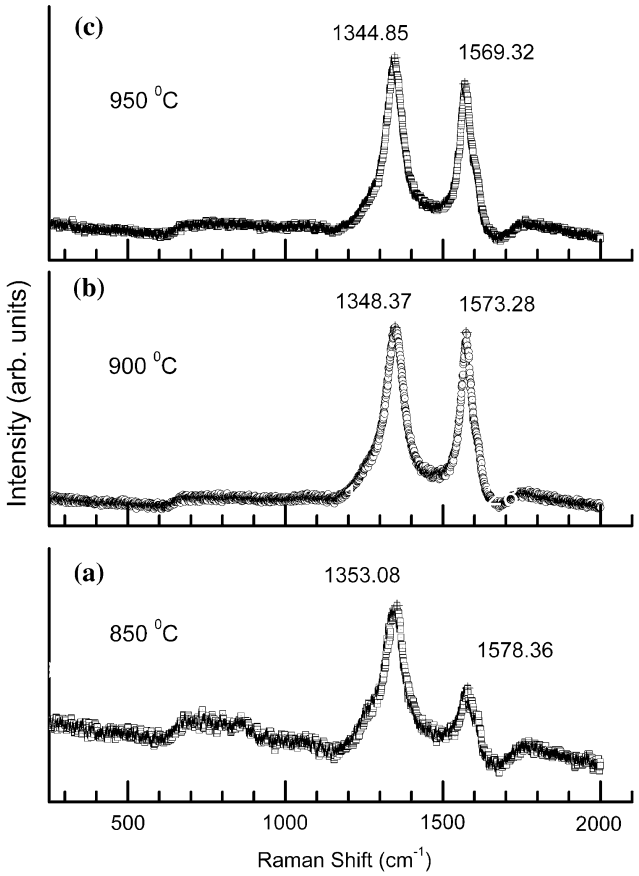

Fig. 5 Raman spectra of C–N nanotubes at different growth temperatures; **a** 850 °C, **b** 900 °C, and **c** 950 °C recorded using 514.5 nm line of Ar-ion laser

The integrated intensity of D mode is usually normalized with respect to that of the G mode for estimating the defect concentration [49, 50]. For C–N nanotubes, differences in chemical bond lengths and atomic masses as well as the formation of pentagons due to the doping of N atoms lead to local distortion in the graphite sheets. So the intensity ratio of the D to G modes (I_D/I_G) is strongly dependent on the defect fraction originating from nitrogen incorporation and could be considered as a measure of the degree of nitrogen hybridization [51, 52]. As the concentration of the N atoms increases, the D-band becomes stronger and broader. The value of I_D/I_G for the N-doped CNTs grown at three temperatures is plotted in Fig. 6. The values of I_D/I_G decrease from ~1.49 to 1.025 as growth temperature increases from 850 to 950 °C (the N content decreases from 8.29 to 3.19%). The data show that the degree of long-range ordered crystalline perfection increases with the temperature and decreases by the N doping. The value of I_D/I_G increases by about 0.4 for the increase in the N content of about 5%. However, almost negligible change was observed in I_D/I_G for CVD grown

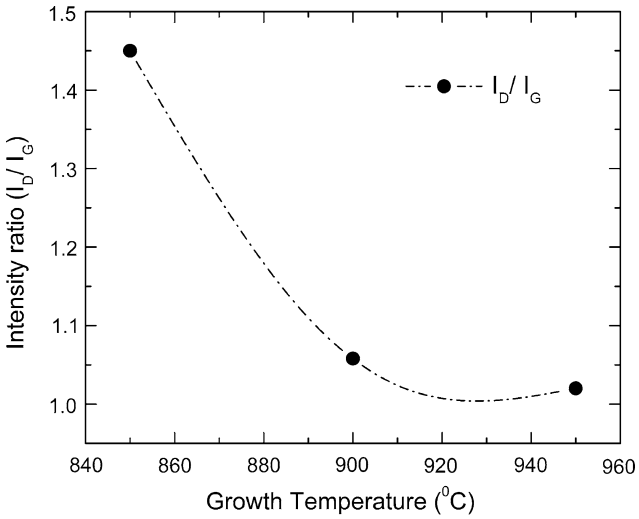

Fig. 6 Variation of Raman intensity ratio of D and G bands (I_D/I_G) at different growth temperatures of nanotubes

C–N nanotubes using pyridine and pyridine + melamine as nitrogen sources [53].

Figure 7 displays the changes of the full width at half-maximum (FWHM) of the D and G bands versus growth temperature, respectively. It is noticed that the FWHM of the D and G bands reduces with increasing growth temperature. This is also evident from the figure that the FWHM of G-band is more influenced by growth temperature than that of the D-band. Their width variations may be taken as a measure of the degree of the disorder (or the concentration of defects). Hence, narrowing of the Raman modes indicates a better crystallization of the nanotubes or a larger crystal planer domain size in graphite sheets and consequently a lower degree of disorder or a lower defect

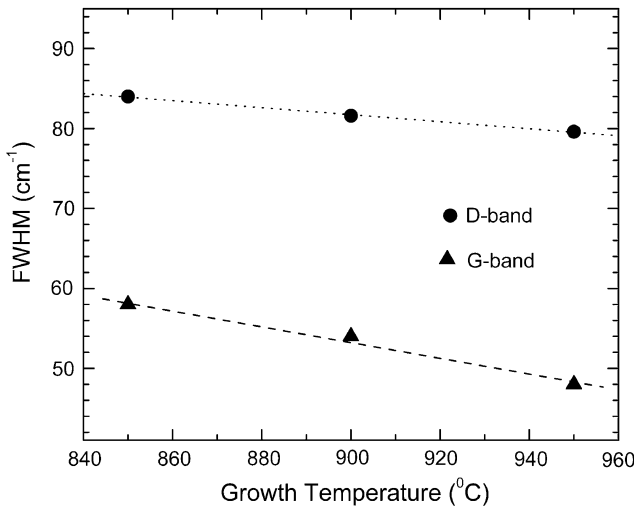

Fig. 7 Variation of FWHM of D and G bands with increasing growth temperature

Table 1 Peak frequencies of Raman D and G mode of C–N nanotubes at three different growth temperatures

Growth temperature (°C)	Peak frequency (cm^{-1})	
	D-mode	G-mode
850	1353.08	1578.36
900	1348.37	1573.28
950	1344.85	1569.32

concentration at higher growth temperature. Moreover, the G-band shifts from ~1578 to 1569 cm^{-1}, whereas the D band shifts from ~1353 to 1344 cm^{-1} (given in Table 1), as the temperature increase from 850 to 950 °C. The amount of shifts correlated to the density of bamboo compartment and consequently to the percentage of N content (or the concentration of defects). The above Raman results show that the degree of disorder and consequently the N hybridization decreases with increasing growth temperature. This is in accordance with TEM and XPS findings.

Conclusions

Our investigations revealed that the percentage (atomic) of nitrogen content in the nanotubes depends on the growth temperature and decreases with increase in temperature. The nanotubes have bamboo-shaped structure for all the growth temperatures. Bamboo compartment distance and the diameter of the nanotubes increase with increasing growth temperature. The FWHMs of the D and G modes reduce linearly with increasing growth temperature. The normalized intensity of the D mode (I_D/I_G) decreases with increasing growth temperature. These are interpreted as increasing in crystal planar domain sizes in graphite sheets and consequently lowering in the defect concentration or the degree of disorder.

Acknowledgments The authors are grateful to Prof. C. N. R. Rao, Prof. P. M. Ajayan, Prof. A. R. Verma, for their encouragement and to Dr. Kalpana Awasthi for helpful discussions. The financial support from DST (UNANST), India is gratefully acknowledged.

References

1. S. Iijima, Nature **354**, 56 (1991). doi:10.1038/354056a0
2. P.M. Ajayan, Chem. Rev. **9**, 1787 (1999). doi:10.1021/cr970102g
3. S.K. Srivastava, V.D. Vankar, V. Kumar, Nanoscale Res. Lett. **3**, 25 (2008). doi:10.1007/s11671-007-9109-x
4. J. Goldberger, R.R. He, Y.F. Zhang, S.W. Lee, H.Q. Yan, H.J. Choi, P.D. Yang, Nature **422**, 599 (2003). doi:10.1038/nature01551
5. R. Tenne, Nat. Nanotechnol. **1**, 110 (2006). doi:10.1038/nnano.2006.62
6. C. Yan, D. Xue, Adv. Mater. **20**, 1055 (2008). doi:10.1002/adma.200701752
7. C. Yan, D. Xue, Electrochem. Commun. **9**, 1247 (2007). doi:10.1016/j.elecom.2007.01.029
8. J. Liu, D. Xue, Adv. Mater. **20**, 2622 (2008). doi:10.1002/adma.200800208
9. D.L. Carroll, P. Redlich, X. Blase, J.-C. Charlier, S. Curran, P.M. Ajayan, S. Roth, M. Rühle, Phys. Rev. Lett. **81**, 2332 (1998). doi:10.1103/PhysRevLett.81.2332
10. W.K. Hsu, S.Y. Chu, E. Muñoz-Picone, J.L. Boldú, S. Firth, P. Franchi, B.P. Roberts, A. Schilder, H. Terrones, N. Grobert, Y.Q. Zhu, M. Terrones, M.E. McHenry, H.W. Kroto, D.R.M. Walton, Chem. Phys. Lett. **323**, 572 (2000). doi:10.1016/S0009-2614(00)00553-4
11. R. Czerw, M. Terrones, J.C. Charlier, X. Blase, B. Foley, R. Kamalakaran, N. Grobert, H. Terrones, D. Tekleab, P.M. Ajayan, W. Blau, M. Ruhle, D.L. Carroll, Nano Lett. **1**, 457 (2001). doi:10.1021/nl015549q
12. D. Golberg, P.S. Dorozhkin, Y. Bando, Z.-C. Dong, C.C. Tang, Y. Uemura, N. Grobert, M. Reyes-Reyes, H. Terrones, M. Terrones, Appl. Phys. A. **76**, 499 (2003). doi:10.1007/s00339-002-2047-7
13. J.-C. Charlier, M. Terrones, M. Baxendale, V. Meunier, T. Zacharia, N.L. Rupesinghe, W.K. Hsu, N. Grobert, H. Terrones, G.A.J. Amaratunga, Nano Lett. **2**, 1191 (2002). doi:10.1021/nl0256457
14. F.J. Owens, Nanoscale Res. Lett. **2**, 447 (2007). doi:10.1007/s11671-007-9082-4
15. M. Terrones, A. Jorio, M. Endo, A.M. Rao, Y.A. Kim, T. Hayashi, H. Terrones, J.C. Charlier, G. Dresselhaus, M.S. Dresselhaus, Mater Today **7**, 30 (2004). doi:10.1016/S1369-7021(04)00447-X
16. M. Yudasaka, R. Kikuchi, Y. Ohki, S. Yoshimura, Carbon **35**, 195 (1997). doi:10.1016/S0008-6223(96)00142-X
17. R. Sen, B.C. Satishkumar, A. Govindaraj, K.R. Harikumar, G. Raina, J.P. Zhang, A.K. Cheetham, C.N.R. Rao, Chem. Phys. Lett. **287**, 671 (1998). doi:10.1016/S0009-2614(98)00220-6
18. K. Jiang, L.S. Schadler, R.W. Siegel, X. Zhang, H. Zhang, M. Terrones, J. Mater. Chem. **14**, 37 (2004). doi:10.1039/b310359e
19. T. de los Arcos, M.G. Garnier, J.W. Seo, P. Oelhafen, V. Thommen, D. Mathys, J. Phys. Chem. B **108**, 7728 (2004). doi:10.1021/jp049495v
20. S. Helveg, C. Lo'pez-Cartes, J. Sehested, P.L. Hansen, B.S. Clausen, J.R.R. Nielsen, F.A. Pedersen, J.K. Nørskov, Nature **427**, 426 (2004). doi:10.1038/nature02278
21. T. de los Arcos, F. Vonau, M.G. Garnier, V. Thommen, P. Oelhafen, M. Düggelin, D. Mathis, R. Guggenheim, Appl. Phys. Lett. **80**, 2383 (2002). doi:10.1063/1.1465529
22. H. Sato, Y. Hori, K. Hata, K. Seko, H. Nakahara, Y. Saito, J. Appl. Phys. **100**, 104321 (2006). doi:10.1063/1.2364381
23. A. Okita, A. Ozeki, Y. Suda, J. Nakamura, A. Oda, K. Bhattacharyya, H. Sugawara, Y. Sakai, Jpn J. Appl. Phys. **45**, 8323 (2006). doi:10.1143/JJAP.45.8323
24. G.Y. Xiong, D.Z. Wang, Z.F. Ren, Carbon **44**, 969 (2006). doi:10.1016/j.carbon.2005.10.015
25. Y.H. Yun, V. Shanov, Y. Tu, S. Subramaniam, M. Schulz, J. Phys. Chem. B **110**, 23920 (2006). doi:10.1021/jp057171g
26. Q.W. Li, X.F. Zhang, R.F. DePaula, L.X. Zheng, Y.H. Zhao, L. Stan, T.G. Holesinger, P.N. Arendt, D.E. Peterson, Y.T.T. Zhu, Adv. Mater. **18**, 3160 (2006). doi:10.1002/adma.200601344
27. M.J. Bronikowski, Carbon **44**, 2822 (2006). doi:10.1016/j.carbon.2006.03.022
28. S.R. Jian, Y.T. Chen, C.F. Wang, H.C. Wen, W.M. Chiu, C.S. Yang, Nanoscale Res. Lett. **3**, 230 (2008). doi:10.1007/s11671-008-9141-5
29. D.N. Futaba, K. Hata, T. Yamada, K. Mizuno, M. Yumura, S. Iijima, Phys. Rev. Lett. **95**, 056104 (2005). doi:10.1103/PhysRevLett.95.056104
30. A. Magrez, J.W. Seo, C. Miko, K. Hernadi, L. Forro, J. Phys. Chem. B **109**, 10087 (2005). doi:10.1021/jp050363r

31. C. Singh, M.S. Shaffer, A.H. Windle, Carbon **41**, 359 (2003). doi:10.1016/S0008-6223(02)00314-7
32. S.K. Srivastava, V.D. Vankar, V. Kumar, V.N. Singh, Nanoscale Res. Lett. **3**, 205 (2008). doi:10.1007/s11671-008-9138-0
33. M. Lin, J.P.Y. Tan, C. Boothroyd, K.P. Loh, E.S. Tok, Y.L. Foo, Nano Lett. **6**, 449 (2006). doi:10.1021/nl052356k
34. R.M. Yadav, T. Shripathi, A. Srivastava, O.N. Srivastava, J. Nanosci. Nanotechnol. **5**, 820 (2005). doi:10.1166/jnn.2005.102
35. R.M. Yadav, A. Srivastava, O.N. Srivastava, J. Nanosci. Nanotechnol. **4**, 719 (2004). doi:10.1166/jnn.2004.105
36. C.J. Lee, S.C. Lyu, H.W. Kim, J.H. Lee, K.I. Cho, Chem. Phys. Lett. **359**, 115 (2002). doi:10.1016/S0009-2614(02)00655-3
37. J.W. Jang, C.E. Lee, S.C. Lyu, T.J. Lee, C.J. Lee, Appl. Phys. Lett. **84**, 2877 (2004). doi:10.1063/1.1697624
38. S. van Dommele, A.R. Izquirdo, R. Brydson, K.P. de Jong, J.H. Bitter, Carbon **46**, 138 (2008). doi:10.1016/j.carbon.2007.10.034
39. S. Hofmann, G. Csanyi, A.C. Ferrari, M.C. Payne, J. Robertson, Phys. Rev. Lett. **95**, 036101 (2005). doi:10.1103/PhysRevLett.95.036101
40. X.F. Zang, X.B. Zang, G.V. Tendelloo, S. Amelinckx, M.O. deBeeck, J.V. Landuyt, J. Cryst. Growth **130**, 368 (1993). doi:10.1016/0022-0248(93)90522-X
41. C.H. Lin, H.L. Chang, C.M. Hsu, A.Y. Lo, C.T. Kuo, Diamond Relat. Mater. **12**, 1851 (2003). doi:10.1016/S0925-9635(03)00209-7
42. Y. Li, B. Zhang, X.Y. Tao, J.M. Xu, W.Z. Huang, J.H. Luo, T. Li, Y. Bao, H.J. Geise, Carbon **43**, 295 (2005). doi:10.1016/j.carbon.2004.09.014
43. P. Tan, L. An, L. Liu, Z. Guo, R. Czerw, D.L. Carroll, P.M. Ajayan, N. Zhang, H. Guo, Phys. Rev. B **66**, 245410 (2002). doi:10.1103/PhysRevB.66.245410
44. L. Liu, Y. Qin, Z.X. Guo, D. Zhu, Carbon **41**, 331 (2003). doi:10.1016/S0008-6223(02)00286-5
45. B.W. Mwakikunga, E.S. Haddad, A. Forbes, C. Arendse, Phys. Status Solidi (a) **205**, 150 (2008). doi:10.1002/pssa.200776829
46. Q. Zhao, H.D. Wagner, Philos. Trans. R. Soc. Lond. A **362**, 2407 (2004). doi:10.1098/rsta.2004.1447
47. G.F. Malgas, C.J. Arendse, N.P. Cele, F.R. Cummings, J. Mater. Sci. **43**, 1020 (2008). doi:10.1007/s10853-007-2230-5
48. G. Katumba, B.W. Mwakikunga, R. Mothibinyane, Nanoscale Res. Lett. **3**, 421 (2008). doi:10.1007/s11671-008-9172-y
49. X.C. Ma, E.G. Wang, R.D. Tilley, D.A. Jefferson, W. Zhou, Appl. Phys. Lett. **77**, 4136 (2000). doi:10.1063/1.1332407
50. L. Zhang, H. Li, K.T. Yue, S.L. Zhang, X. Wu, J. Zi, Phys. Rev. B **65**, 73401 (2002). doi:10.1103/PhysRevB.65.073401
51. E.J. Liang, P. Ding, H.R. Zhang, X.Y. Guo, Z.L. Du, Diamond Relat. Mater. **13**, 69 (2004). doi:10.1016/j.diamond.2003.08.025
52. Y.T. Lee, N.S. Kim, S.Y. Bae, J. Park, S.C. Yu, H. Ryu, H.J. Lee, J. Phys. Chem. B **107**, 12958 (2003). doi:10.1021/jp0274536
53. S. Webster, J. Maultzsch, C. Thomsen, J. Liu, R. Czerw, M. Terrones, F. Adar, C John, A. Whitley, D.L. Carroll, Mater. Res. Symp. Proc. **772**, M7.8.1. (2003)